

# Gaussian Amplitude Amplification for Quantum Pathfinding

Daniel Koch<sup>1,2\*</sup>, Massimiliano Cutugno<sup>2</sup>, Samuel Karlson<sup>3</sup>, Saahil Patel<sup>2</sup>, Laura Wessing<sup>2</sup>, Paul M. Alsing<sup>2</sup>

<sup>1</sup>*The Griffiss Institute, Rome, NY*

<sup>2</sup>*Air Force Research Lab, Information Directorate, Rome, NY*

<sup>3</sup>*Air Force Academy, Colorado Springs, CO and*

*\*Corresponding Author: daniel.koch.10.ctr@afresearchlab.com*

We present a novel quantum Phase Oracle operation, along with its circuit design, which combined with the Grover Diffusion operator boosts the probability of finding minimum / maximum length paths on a weighted geometry. We show that for problems which naturally give rise to solution spaces describable by gaussian distributions, the desired quantum state(s) can achieve boosted probabilities similar to that of Grover's Algorithm. Example Hilbert spaces for this new amplitude amplification process are explicitly shown using classical simulations. And finally, we discuss the strengths and weaknesses of implementing our technique on realistic problem cases which are generated using randomized weighted edges.

## I. INTRODUCTION

The use of quantum computers for tackling difficult problems is an exciting promise, but not one without its own set of challenges. Qubits allows for incredible parallelism in computations via superposition states, but reliably pulling out a single answer via measurements is often a struggle. In 1996, Grover demonstrated one of the first mechanisms overcoming this weakness [1], later shown to be optimal [2, 3], and has since been refined into a broader technique in quantum algorithms known as 'amplitude amplification' [4–9]. In this study we seek to extend the capabilities of amplitude amplification as a means of pathfinding on a weighted geometry.

Upon closer inspection of Grover's Algorithm, the success of the technique can be boiled down to two primary components: the Oracle operation  $U_G$  and Diffusion operation  $U_s$ . While  $U_s$  is typically considered a straightforward mathematical operation, achieving a reflection about the average amplitude, critics of Grover's Algorithm often point to  $U_G$  as problematic [10–13]. Nielsen and Chuang elegantly describe the dilemma of implementing  $U_G$  as differentiating between an operation which *knows* the desired marked state, versus a true blackbox oracle which can *recognize* the answer [14]. Only an oracle of the latter case can truly be considered a speedup for quantum, otherwise the solution to the unstructured search problem is already encoded into  $U_G$ , defeating the purpose of using a quantum computer in the first place. We note this specific issue with Grover's Algorithm because it is exactly the problem we aim to overcome in this study. More specifically, we provide a replacement for the standard Grover Oracle, called a 'Phase Oracle'  $U_P$ , which is able to *recognize* the desired solution state, cause its probability to increase through interference, all while only requiring the base information of a weighted geometry.

Beyond the weighted pathfinding problem used to motivate  $U_P$  and build its corresponding quantum circuit, much of this study is aimed at formulating a deeper understanding of amplitude amplification. The idea of us-

ing an oracle which applies phases different from the standard  $U_G$  was first investigated by Long and Hoyer [15–17] and later others [18–20], who showed the degree to which a phase other than  $\pi$  on the marked state could still be used for probability boosting. Here, we study a  $U_G$  replacement which differs in that it affects *all* states with unique phases, not just a single marked state. The result is an amplification process which is more complex, and yet still impressively able to achieve probabilities that approach 1 under ideal conditions. And most importantly, we demonstrate the degree to which probability boosting is still possible even under randomized conditions which one would expect from realistic optimization problems [21–23].

### A. Layout

The progression of this study revolves around a specific pathfinding problem, where the underlying characteristics of each geometry's solution space are describable by the Central Limit Theorem [24] and the Law of Large Numbers [25], resulting in distributions which resemble a gaussian function [26]. In section II. we begin with specifics of the pathfinding problem, a graphical representation of all possible paths, and a proposed classical solving speed based on arguments of information access. Sections III. and IV. show how the pathfinding problem can be translated into a quantum search algorithm, whereby the natural distribution of all possible paths is used as an advantageous Phase Oracle operator for amplitude amplification. In section V., we outline the viability of using this new oracle operator on more realistic optimization problems involving randomness. Section VI. concludes with a summary of our findings and discussions of future research, such as a theoretical solution to the Traveling Salesman problem[27] .

## II. PATHFINDING GEOMETRY

### A. Geometric Structure

Shown below in figure 1 is the general structure of the geometry which will serve as the primary focus for this study: a series of sequentially connected bipartite graphs with weighted edges, for which the solver is interested in finding the path of least / greatest resistance. The complete structure of each geometry can be specified by two variables,  $N$  and  $L$ , which represent the number of vertices per column and total number of columns respectively. Throughout this study, we will often refer to vertices as ‘nodes’, and each complete set of nodes in a vertical column as a ‘layer’. For example, figure 1’s geometry represents a 4-layer system ( $L = 4$ ), with 3 nodes per layer ( $N = 3$ ).

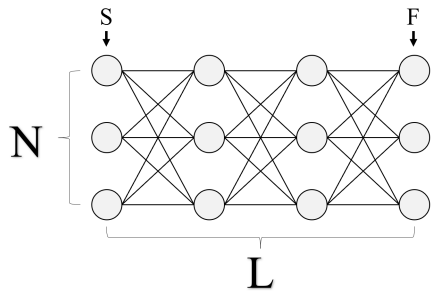


FIG. 1: Geometric structure on which a solver will look to find the shortest / longest path from layer S, to layer F, touching exactly 1 node per layer.  $N$  denotes the number of nodes per layer, while  $L$  is the number of total layers. With full connectivity between nearest neighboring layers (complete bipartite), each geometry has a total of  $N^2 \cdot (L - 1)$  edges, yielding  $N^L$  possible paths from layer  $S$  to  $F$ .

Given the geometric structure shown above, we now assign a complete set of weights  $\omega_i$ , one for each of the total  $N^2 \cdot (L - 1)$  edges throughout the geometry. Given this complete set of weights, we now task a solver with finding the either the minimum or maximum length path ( $W_{\min}$  or  $W_{\max}$ ), defined below in equations 1-6, where  $W_j$  is the sum of all weighted edges  $w_i$  that make up a single path  $P_j$ :

$$\omega_i \in [1, R], \quad \omega_i \in \mathbb{Z} \quad (1)$$

$$W_j = \sum_{i \in P_j} \omega_i \quad (2)$$

$$\mathbb{P} \equiv \{P_1, P_2, \dots, P_{N^L}\} \equiv \text{All Paths} \quad (3)$$

where the smallest / largest  $W_j$  values correspond to the desired solutions:

$$\mathbb{W} \equiv \{W_1, W_2, \dots, W_{N^L}\} \equiv \text{All Path Weights} \quad (4)$$

$$W_{\min} \leq x, \quad x \forall \mathbb{W} \quad (5)$$

$$W_{\max} \geq x, \quad x \forall \mathbb{W} \quad (6)$$

For clarity, a single path  $P_j$  is defined as the collection of edges which span from the leftmost to rightmost layers, touching exactly one node in every layer. For example, each path in figure 1 connects exactly 4 nodes between layers S and F, touching one of the 3 nodes per layer, for a total of 81 possible paths (also see figure 2 below).

### B. Classical Solving Speed

As outlined in equations 1-6, the goal of the solver is to find either  $W_{\min}$  or  $W_{\max}$ , the smallest or largest  $W_j$  value within the set  $\mathbb{W}$ . Presented in this way, the problem mathematically resembles that of an unstructured search through  $\mathbb{W}$  of size  $N^L$ , for which the classical solving speed is  $O(\frac{1}{2}N^L)$ . However, because the population of  $\mathbb{W}$  is produced from the geometric structure of figure 1, a more optimal solution turns out to be  $O(N^2 \cdot (L - 1))$ . Figure 2 below is an example of how an optimal classical algorithm solves the pathfinding problem one layer at a time.

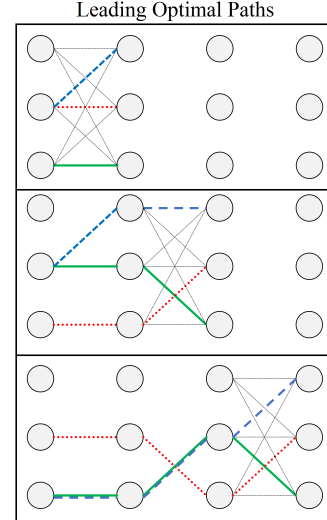


FIG. 2: A layer by layer example of an optimal classical approach to finding  $W_{\min}$  or  $W_{\max}$ , for the case of  $N = 3$  and  $L = 4$ . The blue-dashed, green-solid, and red-dotted lines each represent possible solutions for the optimal path ending on each of the three nodes per layer.

The strategy illustrated in figure 2 can be summarized as the recursive process given in algorithm 1. The emphasized edges (dashed, dotted, bolded) throughout figure 1 represent the  $N = 3$  leading candidates for the optimal path, up to each layer. Importantly, the algorithm requires that each candidate path end on a different node, in anticipation for the next  $N^2$  edges in the coming layer. At each step of the algorithm, these  $N$  candidate paths are used to determine the next  $N$  candidates, repeating this process up to the final layer.

It is not coincidental that the proposed optimal solving speed shown above is exactly equal to the number of

**Algorithm 1** Classical Pathfinding

---

```

1: OP = { 0, 0, ..., 0 } (length  $N$ )
2: while  $i \leq L - 1$  do
3:   while  $j \leq N^2$  do
4:     Check edge weight  $w_{i,j}$ 
5:     Compute if  $OP_k + w_{i,j}$  is optimal
6:     if Yes then
7:       Replace  $OP_k$ 
8:    $W_{\min/\max} = \min/\max OP$ 

```

---

total edges in the system. From an information resource perspective, we argue that this is classical limit, in that any optimal algorithm for finding  $W_{\min}$  or  $W_{\max}$  must use the information of each edge's weight at least once. Under certain circumstances, such as *a priori* knowledge of  $\omega_i$ 's bounds like in equation 1, a slightly more optimal solution could in theory ignore edges nearing the end of the algorithm. However, these cases are problem specific, and thus in this study we shall regard  $O(N^2 \cdot (L - 1))$  as the solving speed to beat for any quantum algorithm.

### III. QUANTUM PHASE ORACLE

Having now outlined the pathfinding problem of interest, as well as arguments for its classical solving limit, in this section we present the quantum strategy for pathfinding. We begin by outlining the manner in which all  $N^L$  possible paths are uniquely assigned a quantum state, with the goal of encoding each total path length  $W_i$  via phases. Then later in section IV., we show how these phases can be used for amplitude amplification in order to learn  $W_{\min}$  or  $W_{\max}$ .

#### A. Representing Paths in Quantum

As is typical when using qubits, the methodology put forth in this study is most naturally suited to problem sizes where  $N = 2^n$  (nodes per layer). As a side note, geometries of size  $N \neq 2^n$  can be adapted up to the nearest  $N = 2^{n'}$  value by repeating nodes and edges, for which all of the results to come then become applicable, but at the cost of solving speed. We begin by presenting two example cases in figure 3 of size  $N = 2$  and  $N = 4$ , both  $L = 4$ . Accompanying each geometry are the qubit states needed to represent each node per layer.

Because we are interested in a quantum pathfinding problem, the manner in which the qubits' orthogonal basis states  $|0\rangle$  and  $|1\rangle$  are used need to reflect this fact. That is to say, a final measurement at the end of the algorithm will yield all  $|0\rangle$ 's and  $|1\rangle$ 's, from which the solver must then extrapolate its corresponding path, which we refer to as  $|P_i\rangle$ . We achieve this by encoding the meaning of each qubit state as the location of a particular node in the geometry. Using  $\sqrt{N}$  qubits allows us to identify each of the  $N$  nodes per layer, for a total of  $\sqrt{N} \cdot L$

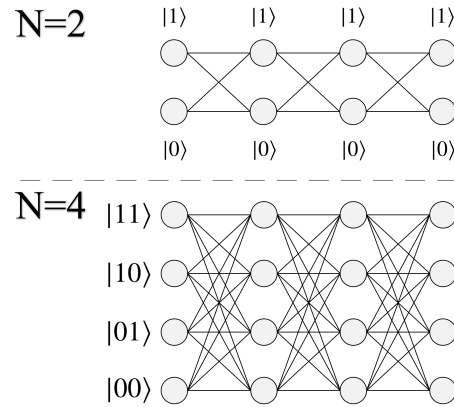


FIG. 3: (top) An example geometry of size  $N = 2$ ,  $L = 4$ . For the case of  $N = 2$ , a single qubit is sufficient for representing all possible node choices per layer via the states  $|0\rangle$  and  $|1\rangle$ . (bottom) An example geometry of size  $N = 4$ ,  $L = 4$ , where now two qubits are necessary for representing the nodes in each layer.

qubits representing the complete geometry. Importantly, the manner in which qubits are grouped together is necessary for decoding a particular path from its  $|P_i\rangle$  state, such as in figure 3 where two qubit states are used to indicate one of four possible nodes per layer. Figure 4 below shows an example path for the  $N = 2$  geometry, and its corresponding  $|P_i\rangle$ . With quantum states encoded in this manner, it then follows that the ultimate goal of the algorithm is to measure  $|P_{\min}\rangle$  /  $|P_{\max}\rangle$ , which will yield the answer  $W_{\min}$  /  $W_{\max}$ .

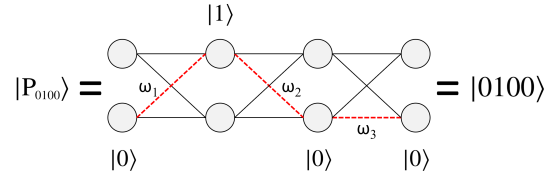


FIG. 4: An example path (red-dashed) for a geometry of size  $N = 2$ ,  $L = 4$ . The quantum state  $|0100\rangle$  represents the path shown in red, using the single qubit states  $|0\rangle$  and  $|1\rangle$  for bottom and top row nodes respectively.

#### B. Phase Oracle $U_P$

While the state shown in figure 4 corresponds to a single path, it then follows that a superposition state of size  $N^L$  can be used to represent all possible paths simultaneously. And in order to use these states for pathfinding, a mechanism for assigning each path state  $|P_i\rangle$  its unique path weight  $W_i$  is necessary. To achieve this, we propose an operation  $U_P$ , which we refer to as a 'Phase Oracle', capable of applying the cumulative weights  $W_i$  of each path through phases:

$$\begin{aligned}
U_P |0100\rangle &= (e^{i\omega_1} \cdot e^{i\omega_2} \cdot e^{i\omega_3}) |0100\rangle \\
&= e^{i(\omega_1 + \omega_2 + \omega_3)} |0100\rangle \\
&= e^{iW_{0100}} |0100\rangle
\end{aligned} \tag{7}$$

In equation 7 above, we've used the numerical weights  $\omega_i$  from figure 4 as an example, whereby each edge is directly translated into a phase contribution. In practice however, a scaling factor  $p_s$  is necessary for meaningful results (which we discuss in section IV.). Nevertheless, the vital component here for our quantum approach is the Phase Oracle operator  $U_P$ . The matrix representation of  $U_P$  has the form of equation 8 below, acting on the standard binary basis states, where each phase  $\phi_i$  is a scalar of the form  $p_s \cdot W_i$ . The matrix for  $U_P$  has dimensions  $N^L \times N^L$ , equal to the total number of paths, with each path's unique phase along the main diagonal.

$$U_P |\Psi\rangle = \begin{bmatrix} e^{i\phi_0} & 0 & 0 & \dots \\ 0 & e^{i\phi_1} & 0 & \\ 0 & 0 & e^{i\phi_2} & \\ \vdots & & \ddots & \end{bmatrix} \begin{bmatrix} |0000\rangle \\ |0001\rangle \\ |0010\rangle \\ \vdots \end{bmatrix} \tag{8}$$

It is important to note that the matrix shown in equation 8 is *not* necessary for the actual implementation of  $U_P$ . In particular, computing all  $N^L$  phases is already slower than the  $O(N^2 \cdot (L - 1))$  approach laid out in section II., which is analogous to the discussion about  $U_G$  from the Introduction section. Thus, as we demonstrate in the next subsection, a viable quantum approach needs to implement  $U_P$  *without* calculating any total path lengths  $W_i$ .

### C. Quantum Circuit

Having now seen the desired effect from  $U_P$  (equation 8), here we present a quantum circuit design which efficiently achieves all  $N^L$  unique phases, with no *a priori* classical computations of  $W_i$ . Once again, we will focus on the case  $N = 2$  for simplicity, leaving the general case for a later discussion (also see Appendix A for the  $N = 4$  circuit). We begin by defining the operator  $U_{ij}$  shown below in equation 9, and its corresponding quantum circuit in figure 5, which encodes all of the phases contained between layers  $i$  and  $j$ , illustrated for the  $N = 2$  case.

$$U_{ij} \equiv \begin{bmatrix} e^{i\phi_{00}} & 0 & 0 & 0 \\ 0 & e^{i\phi_{01}} & 0 & 0 \\ 0 & 0 & e^{i\phi_{10}} & 0 \\ 0 & 0 & 0 & e^{i\phi_{11}} \end{bmatrix} \tag{9}$$

The circuit shown in figure 5 applies a unique phase to each of the 2-qubit quantum states  $|Q_i Q_j\rangle$ , corresponding

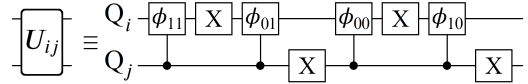


FIG. 5: Quantum circuit for achieving the  $U_{ij}$  operation outlined in equation 9.

to each of the four edges connecting layers  $i$  and  $j$ . Note that the complete information of all edges connecting layers  $i$  and  $j$  can be achieved with exactly one phase gate (controlled) per edge, which is a property that holds true for all geometry sizes. From a connectivity view point, this means that the qubits which make up layer  $i$  only need to interact with the qubits making up layers  $i \pm 1$ . This in turn can be used to significantly reduce circuit depth, demonstrated below in figure 6.

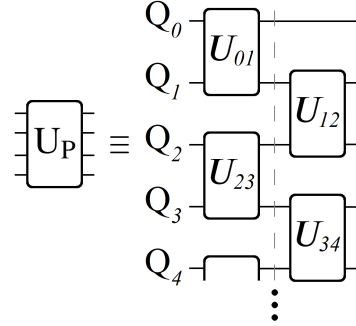


FIG. 6: The complete circuit design for  $U_P$ , for the case of  $N = 2$ . Each  $U_{ij}$  operation applies the four  $\phi_i$  phases corresponding to the  $\omega_i$  weights connecting layers  $i$  and  $j$ . Because of the way in which phases add exponentially, the order in which a total weight  $W_i$  is applied to a state  $|P_i\rangle$  can be done in two sets of parallel operations, shown by the dashed-grey line.

We would like to stress that the structure of figure 6 is general for all geometry sizes. The parameter  $N$  dictates the number of qubits needed per layer, which in turn determines the qubit inputs for  $U_{ij}$ . But the parameter  $L$  (geometry length) has no impact on circuit depth, as the complete implementation of  $U_P$  can always be achieved through two sets of  $U_{ij}$ 's, shown by the dashed-grey line. And most importantly, note that nowhere in circuits 5 and 6 did we compute any of the  $W_i$  path lengths. Instead, we let each  $U_{ij}$  operation apply one  $\omega_i$  component at a time, taking advantage of the way in which phases multiply exponentially, exactly like shown in equation 7. For more details on circuit design, and examples of viability on IBM's superconducting qubits, see Appendixes A and B.

### D. Why An Oracle?

As alluded to in the Introduction section, it is important to note why we've chosen to call  $U_P$  an 'oracle' operation. In the next two sections we showcase the effective-

ness of  $U_P$  as a means for amplitude amplification when used in conjunction with the Grover Diffusion operator  $U_s$ , replacing the standard Grover Oracle operator  $U_G$ . More generally however, we believe that  $U_P$  satisfies the two conditions which must hold true for any quantum operation considered to be an oracle: 1)  $U_P$  can mark the quantum states corresponding to the shortest / longest paths with unique phases (shared by no other states in the system), while 2) requiring no *a priori* information / calculations for the implementation of the quantum circuit beyond simply the weighted edges of the problems  $\omega_i$ .

#### IV. QUANTUM PATHFINDING

With the mechanics of  $U_P$  outlined in section III., here we discuss how this Phase Oracle operator can be used to solve a minimum / maximum path length problem on geometries like in figure 1. Because  $U_P$  is able to mark each quantum state with a unique phase, proportional to the path's  $W_i$ , we demonstrate how the complete set of all path lengths  $\mathbb{W}$  can be used for amplitude amplification.

##### A. Naturally Gaussian

The motivation for studying the geometry shown in figure 1 is in part due to its efficient circuit implementation (see figures 5 and 6), but also the way in which it distributes total path lengths  $W_i$ . More specifically, we consider the case where each weighted edge  $\omega_i$  in the geometry is an integer value chosen from the same uniform random distribution, shown in equation 1. As either  $N$  or  $L$  increases, particularly  $L$ , the statistically expected range of possible solutions becomes increasingly ‘gaussian-like’, where the majority of path lengths cluster around the expected mean  $\mu \approx \frac{R}{2}(L - 1)$ . Consequently, these larger sized problems become increasingly approximatable by the Law of Large Numbers (‘LLN’) [25] and Central Limit Theorem [24] (‘CLT’), resulting in distributions that best fit a gaussian, shown in equation 10.

$$G(x) = \alpha e^{\frac{(x-\mu)^2}{2\sigma^2}} \quad (10)$$

Figure 7 illustrates a few example problem sizes for various  $N$  and  $L$ , and their resulting  $\mathbb{W}$  distributions. By restricting each  $\omega_i$  weight to be an integer value, with a sufficiently small enough  $R$  range (but still large enough to ensure a single  $W_{\min}$  or  $W_{\max}$ ), the result is many duplicate  $W_i$  path lengths through the geometry. Simultaneously, the tail ends of the distribution represent our desired states  $|P_{\min}\rangle$  and  $|P_{\max}\rangle$ , which do not share the same total path length with any other state in the system. As we shall see, it is the combination of these two factors that will yield successful amplitude amplifications.

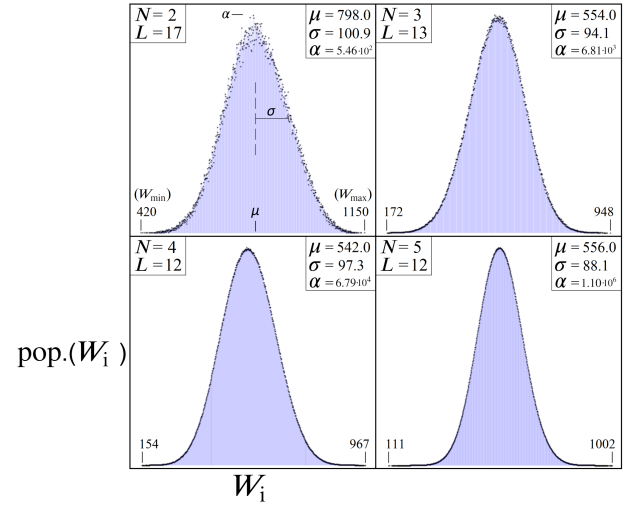


FIG. 7: Histograms of  $W_i$  for randomly generated weighted geometries of various  $N$  and  $L$  sizes, with  $R = 100$ . As  $N$  and  $L$  increase, the profile of these  $\mathbb{W}$  distributions approach perfect gaussians, given in equation 10.

##### B. Mapping to $2\pi$

When using a Phase Oracle operation as defined in equation 8, it is important to note that  $U_P$  does not only mark the states corresponding to  $W_{\min}$  /  $W_{\max}$ , but *all* states uniquely. This is quite different from the standard Grover Oracle  $U_G$ , which *only* marks the state(s) of interest and nobody else. And for this reason, it can be said then that the power of  $U_P$  for amplitude amplification is less flexible than  $U_G$ . While  $U_G$  can in principle be used to boost any of the  $N^L$  quantum states in  $|\Psi\rangle$ ,  $U_P$  on the other hand is better suited for boosting a much smaller percentage of states. However, the states which  $U_P$  is effective at boosting are  $|P_{\min}\rangle$  and  $|P_{\max}\rangle$ , perfect for a pathfinding algorithm.

In viewing the  $\mathbb{W}$  histograms in figure 7, let us now consider the effect of applying such a  $U_P$  operation on an equal superposition state  $|s\rangle$  (step 2 in Algorithm 2). Each point along the x-axis corresponds to a particular path length  $W_i$ , while the y-axis represents the total number of quantum states which will receive a phase proportional to that weight:  $e^{iW_i}|P_i\rangle$ . Thus, the net result of  $U_P$  will apply all  $N^L$  phases in this gaussian-like manner, with the majority of states near the mean receiving the same total phase, regardless of their contributing  $\omega_i$ 's. And now, in order to capitalize on this distribution of phases, we will introduce a phase scaling constant  $p_s$  into the oracle operation, which will affect all states equally:

$$U_P(p_s)|\Psi\rangle = \sum_j^{N^L} e^{ip_s W_j} |P_j\rangle = e^{ip_s} U_P |\Psi\rangle \quad (11)$$

The scaling constant  $p_s$  is nothing more than a global

phase, but it is necessary for amplitude amplification to be successful. Alternatively, it can be thought of as simply the translation of any problem's  $\mathbb{W}$ , for any scale of numbers used, into a regime of phases which can be used for boosting. More specifically, a range of  $[x, x + 2\pi]$  for which the state  $|P_{\min}\rangle$  or  $|P_{\max}\rangle$  is optimally spaced away from the center of the gaussian (depending on which one the solver is looking for). See figure 9 for an illustrated example, and note the location of the red 'x' in the complex plane corresponding to  $|\Psi\rangle$ 's collective mean after  $U_P$ .

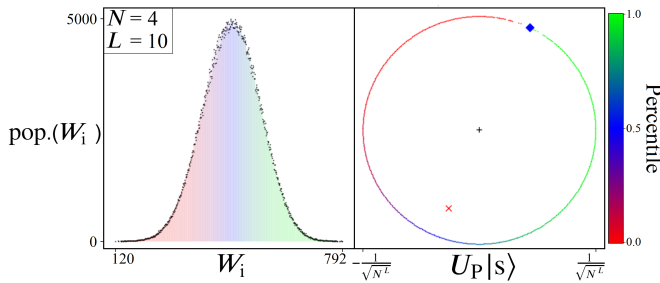


FIG. 8: (left) An example distribution of all  $W_i$  paths for the case of  $N = 4$ ,  $L = 10$ ,  $R = 100$ . (right) The same distribution mapped to a complete  $2\pi$  cycle of phases via the Phase Oracle  $U_P$ , after acting on the equal superposition state  $|s\rangle$ . Additionally, the resulting mean (red 'x') and  $|P_{\min}\rangle / |P_{\max}\rangle$  states (blue diamond) are shown. An accompanying color scale is provided on the far right, illustrating the percentile distribution of states for both plots.

Without  $p_s$ , the weighted paths which make up a given  $\mathbb{W}$  distribution have no guarantee of producing any meaningful amplitude amplification. However, when scaled properly with an optimal  $p_s$  (which is discussed in section V.),  $U_P$  can be made to distribute phases like shown in figure 8, where the phases picked up by  $|P_{\min}\rangle$  and  $|P_{\max}\rangle$  form a range of  $[x, x + 2\pi]$ . This in turn ensures that the majority of states will cluster near  $x + \pi$ , pulling the amplitude mean (red 'x') away from  $|P_{\min}\rangle$  and  $|P_{\max}\rangle$  (blue diamond).

### C. $U_G$ vs $U_P$ Diffusion

As with the standard Grover Search Algorithm [1], the  $U_P$  oracle operation in isolation is not enough to solve for  $W_{\min}$  or  $W_{\max}$ . A second mechanism for causing interference is necessary in order to boost the probability of measuring the desired state. For this, we use the standard Grover Diffusion operator  $U_s$ , given in equation 12:

$$U_s = 2|s\rangle\langle s| - \mathbb{I} \quad (12)$$

where  $|s\rangle$  is the equal superposition state (all positive), and  $\mathbb{I}$  is the identity operator. With  $U_P$  phase tagging each state, and  $U_s$  causing reflections about the average,

---

### Algorithm 2 Quantum Pathfinding

---

- 1: Initialize Qubits:  $|\Psi\rangle = |0\rangle^{\otimes N}$
- 2: Prepare Equal Superposition:  $H^N|\Psi\rangle = |s\rangle$
- 3: **for**  $k \approx \sqrt{N^L}$  **do**
- 4:     Apply  $U_P|\Psi\rangle$  (Phase Oracle)
- 5:     Apply  $U_s|\Psi\rangle$  (Diffusion)
- 6: **Measure**

---

we now have the sufficient tools for quantum pathfinding, shown in algorithm 2.

Perhaps unsurprisingly, the algorithm outlined here is almost exactly that of Grover's Search Algorithm, with  $U_G$  swapped out for  $U_P$ . However, this replacement has dramatic consequences on the way in which the states of  $|\Psi\rangle$  go through amplitude amplification, and remarkably still yields probabilities that approach 1 for large problem sizes.

Figure 9 showcases what amplitude amplification looks like using  $U_P$ , or more generally a gaussian phase distribution. For a comparison, the amplitude space when using the standard  $U_G$  is plotted below. Step 1 illustrates the effect of using the diffusion operator  $U_s$  immediately following the first application of  $U_P$  (see figure 8). As pointed out, the location of the mean point (red 'x') causes states near  $|P_{\min}\rangle / |P_{\max}\rangle$  (blue diamond) to reflect further, increasing their probability (distance from the origin squared). However, this increase will always be smaller than that of standard Grover amplitude amplification, which can be seen in the probabilities shown below each plot in figure 9. Geometrically, this is a consequence of having states spread out over a  $2\pi$  range, resulting in a mean point which is closer to the origin as compared to standard Grover's.

What follows after step 1 for the case of  $U_P$  is a process with no simple mathematical description. As illustrated in steps 2 - 5, repeat applications of  $U_P$  and  $U_s$  result in quantum superposition states which exhibit a 'spiralizing' effect around the mean point. Comparatively, both amplitude amplification processes causes the mean point to move closer towards the origin with each iteration, up to some step of maximal probability for the desired state ( $O(\sqrt{N^L})$  for Grover's). However, because  $U_P$  applies phases over a complete  $2\pi$  range, states nearest to the center of the gaussian are the first to spiral around the mean point. Simultaneously, states near  $|P_{\min}\rangle / |P_{\max}\rangle$  (blue diamond) stay distanced from the mean, and consequently are the last to spiral inwards. But most importantly, when scaled with a proper  $p_s$ ,  $|P_{\min}\rangle / |P_{\max}\rangle$  can be made to perfectly align with the moving mean point and origin, avoiding spiraling inwards, ultimately achieving peak probabilities comparable to that of standard Grover's.

Through many simulated gaussian-like  $\mathbb{W}$  distributions, and their resulting amplitude amplifications, we conclude that the process illustrated in figure 9 is general, which we refer to as 'gaussian amplitude amplification'. When performed using  $\mathbb{W}$  distributions discretized

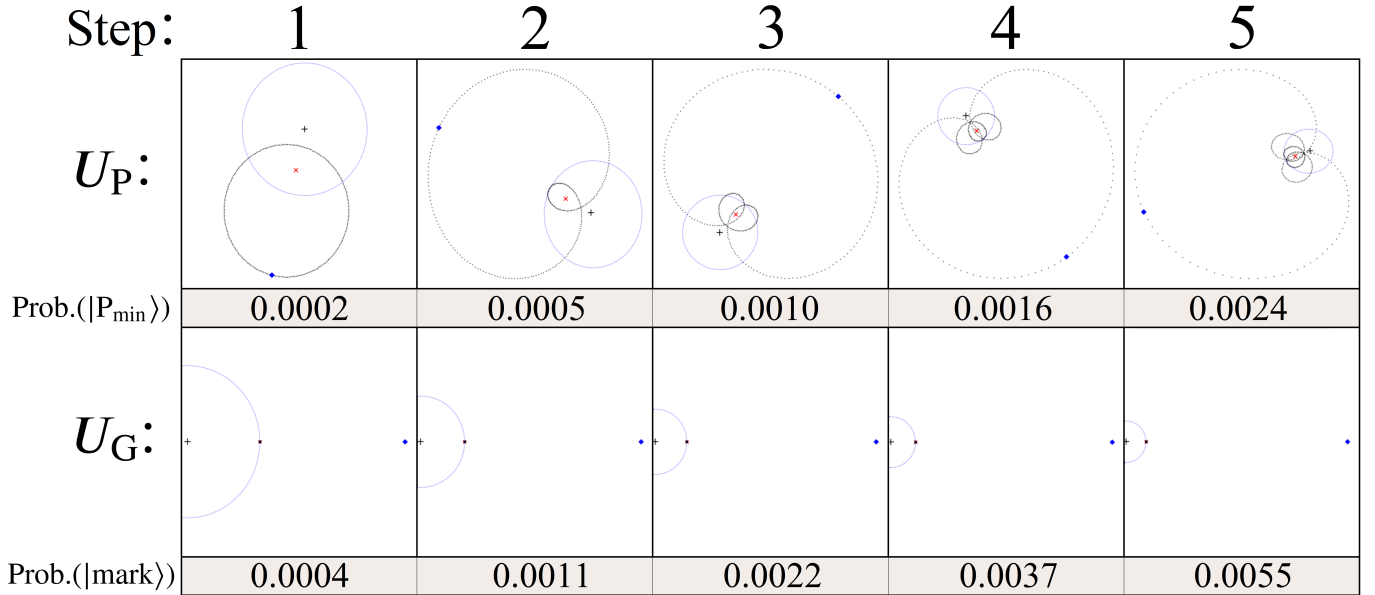


FIG. 9: Examples of amplitude amplification, comparing the use of  $U_P$  vs.  $U_G$  for five iterations, both with the same number of total states  $N' = 24,000$ . In both plots, the origin  $(0,0)$  (black '+'), the mean point (red 'x'), the desired boosted state (blue diamond), and all other points (black circles) are shown. For scale, the radius of the equal superposition state  $|s\rangle$  (blue circle) is also shown ( $1/\sqrt{N'}$ ), as well as the probability of measuring the blue diamond state (which can be used to infer distance to the origin).

from perfect gaussians (no random deviations), we find achievable boosts in probability to  $|P_{\min}\rangle / |P_{\max}\rangle$  of over 99.9%, depending on factors such as the scale of  $N^L$ , the distance of  $W_{\min} / W_{\max}$  from  $W_{\text{mean}}$ , and the standard deviation of the distribution  $\sigma$ . And critically, these optimal boost cases only require iterations on the order of  $O(\sqrt{N^L})$ , similar to Grover's, making them viable for quantum speedups.

#### A. Finding an optimal $p_s$

We begin by presenting a sample  $\mathbb{W}$  distribution (randomly generated), given in figure 10 below, from which several upcoming results are based upon. The parameters  $N = 6$  and  $L = 10$  were chosen in order to showcase a problem size large enough where the LLN and CLT are both relevant, totaling a Hilbert Space of roughly over 60 million states ( $\sim 7770$  qubits), while still possessing enough randomness to cause difficulties for a solver. Also plotted alongside the  $\mathbb{W}$  distribution is a gaussian best-fit, minimizing the correlation parameter given in equation 13.

## V. ALGORITHMIC VIABILITY

It is important to restate that the results shown in figure 9, and the claimed achievable 99.9 % peak probabilities, are based on  $\mathbb{W}$  distributions which were artificially created from perfect gaussians 10. Consequently, these cases should be thought of as the theoretical upper limit for gaussian amplitude amplification. But now, we ask how reliable this boosting mechanism is for  $\mathbb{W}$  distributions more akin to figure 7, with imperfections that one would expect from realistic problems. What follows in the coming subsections are observations and techniques for applying the quantum pathfinding algorithm 2 to randomly generated  $\mathbb{W}$  distributions according to equations 1 - 6.

$$\begin{aligned} Y_i &= \text{pop.}(W_i) & Y'_i &= G(W_i) \\ R_{\text{corr}} &= \sqrt{\frac{\sum_i (Y'_i - \bar{Y})^2}{N^L}} \end{aligned} \quad (13)$$

In order to achieve a successful gaussian amplitude amplification on  $|P_{\min}\rangle / |P_{\max}\rangle$ , even with imperfect  $\mathbb{W}$  distributions, the key lies in finding an optimal scaling parameter  $p_s$ . In section IV.B. we noted that  $p_s$  was necessary in order to translate the full range of  $\mathbb{W}$  down to  $[x, x + 2\pi]$ , which in turn causes the phases picked up by  $|P_{\min}\rangle / |P_{\max}\rangle$  to be roughly  $\pi$  different from states near the center of the gaussian.

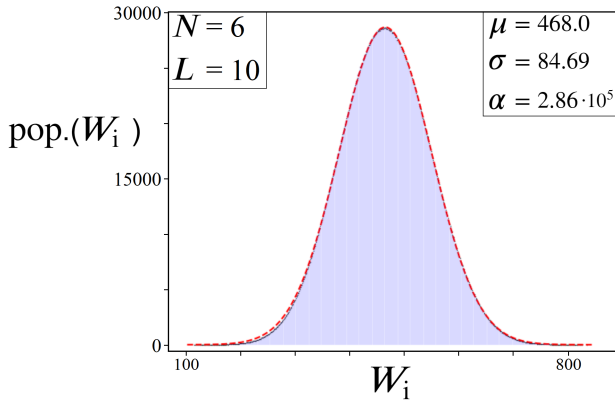


FIG. 10: (black circles / blue lines) A histogram of a randomly generated  $\mathbb{W}$  distribution, for  $N = 6$ ,  $L = 10$ ,  $R = 100$ . (red dash) A best-fit gaussian plot of the form given in equation 10, minimizing equation 13, with parameter values reported in the top-right .

$$\begin{aligned} W_{\min} \cdot p_s &= x \\ W_{\max} \cdot p_s &= x + 2\pi \\ p_s &= \frac{2\pi}{W_{\max} - W_{\min}} \end{aligned} \quad (14)$$

The approach outlined in equation 14 can be thought of as a way of ensuring  $|P_{\min}\rangle$  and  $|P_{\max}\rangle$  both receive the same net phase contribution, but it's not necessarily the optimal  $p_s$  for amplitude amplification. When working with an imperfect  $\mathbb{W}$  distribution, such as figure 10, the optimal  $p_s$  for boosting  $|P_{\min}\rangle$  will differ from  $|P_{\max}\rangle$ . Figure 11 illustrates this point, as well as the margin for error in finding the optimal  $p_s$ , showcasing a range of  $p_s$  values around where  $|P_{\min}\rangle$  can be optimally boosted, along with the second lowest solution state  $|P'_{\min}\rangle$ .

The plots shown in figure 11 were put together by carefully simulating algorithm 2 over the range of  $p_s$  values shown, for  $|P_{\min}\rangle$  as well as the second best solution state  $|P'_{\min}\rangle$ . It is clear by the two spikes in probability, and the space in between, that the role of  $p_s$  for unlocking successful amplitude amplifications cannot be ignored. For this example based on figure 10, using a scaling factor of  $p_s \approx 0.0089569$  causes the state  $|P_{\min}\rangle$  to reach a peak probability of about 80.37%, while using  $p_s \approx 0.0089823$  causes  $|P'_{\min}\rangle$  to boost to about 80.47%. Thus, a margin of error on the order of  $\sim 3 \cdot 10^{-5}$  in  $p_s$  is enough to change what state gets boosted.

The noteworthy takeaways from figure 11 can be summarized as follows: 1) Despite there being a single optimal  $p_s$  for boosting  $|P_{\min}\rangle$ , the plot shows that there is still a range of  $p_s$  values around the optimal case for which the algorithm can still be successful, shown by the width of the two peaks. 2) The range of  $p_s$  values between the two peaks can be regarded as a 'dead zone', for which no state in the system receives a meaningful probability boost. 3) Because states near  $|P_{\min}\rangle$  are also able

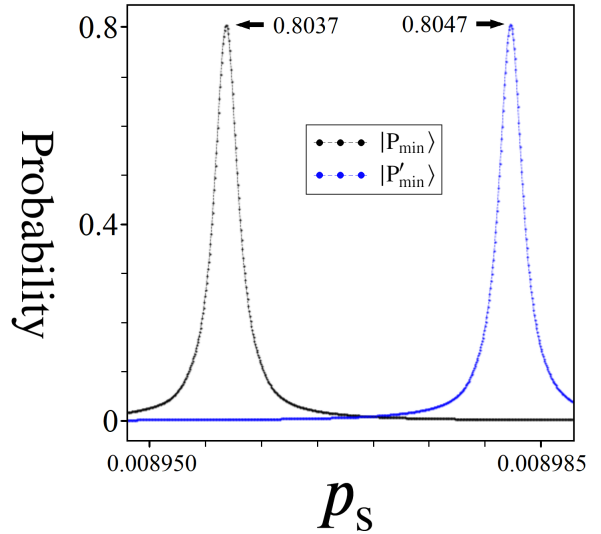


FIG. 11: A plot of  $p_s$  vs achievable probabilities via amplitude amplification, for the  $\mathbb{W}$  distribution shown in figure 10. The state  $|P_{\min}\rangle$  represents the solution to the pathfinding problem  $W_{\min}$ , while  $|P'_{\min}\rangle$  corresponds to the next smallest  $W_i$ .

to receive meaningful amplitude amplifications, this suggests that quantum may be usable as a heuristic approach for pathfinding. 4) From an experimental viewpoint, the scale of precision shown for  $p_s$  must be achievable via phase gates, which means that the size of implementable problems will be dictated by the technological limits of state-of-the-art quantum devices and their error thresholds.

## B. Single vs. Multiple $p_s$

The plots shown in figure 11 represent potential amplitude amplification peaks, where a single  $p_s$  scaling factor is used for every iteration of  $U_s U_P$ . However, in principle this is not necessarily the optimal strategy for boosting  $|P_{\min}\rangle$ , as  $p_s$  could theoretically be different with each iteration. This choice in  $p_s$  is an extra degree of freedom as compared to  $U_G$ , which notably is already optimal in the way marked/unmarked states receive phases (see figure 9). The motivation for studying a step-varying approach to  $p_s$  is to better understand its potential for handling randomness in  $\mathbb{W}$ .

In order to better quantify the advantage a step-varying  $p_s$  approach has to offer, let us first define our metric for a successful amplitude amplification in equation 15 below. We refer to this metric as 'Probability of Success', labeled  $P_{\text{succ}}$ , which combines an amplitude amplification's peak probability and step count into a single number, quantifying the probability of a quantum speedup over classical.

$$\begin{aligned}
C_{\text{steps}} &= N^2 \cdot (L - 1) \\
r &= \lfloor C_{\text{steps}} / Q_{\text{steps}} \rfloor \\
P_M &= \text{Prob.}(|P_{\min}\rangle) \\
P_{\text{succ}} &= 1 - (1 - P_M)^r
\end{aligned} \tag{15}$$

To summarize the components making up equation 15:  $C_{\text{steps}}$  is the number of classical steps needed to find  $W_{\min}$  (equal to the total number of edges),  $Q_{\text{steps}}$  is the number of  $U_s U_P$  iterations needed in order to reach the peak probability  $P_M$ , and  $r$  is the number of allowable amplitude amplification attempts to measure  $|P_{\min}\rangle$  before exceeding  $C_{\text{steps}}$ . Altogether,  $P_{\text{succ}}$  represents the probability that  $|P_{\min}\rangle$  will be successfully measured within  $r$  attempts. Using dice as a simple example, the Probability of Success that one will roll a 1-5 in four attempts is  $P_{\text{succ}} = 1 - (1 - \frac{5}{6})^4 \approx 99.92\%$ .

The quantity  $P_{\text{succ}}$  is a simplified way of comparing quantum vs. classical speeds, more specifically query complexity, which ignores many of the extra complicating factors of a more rigorous speed comparison (classical CPU speeds, quantum gate times, quantum decoherence and fault tolerance, etc.). Here, we are simplifying one step in classical as the processing of information from a single weighted edge  $\omega_i$  (steps 4-7 in Alg. 1), versus one step in quantum as an iteration of  $U_s U_P$  (steps 4 & 5 in Alg. 2). This is the traditional manner in which Grover's Algorithm is considered a quadratic speedup, and is sufficient for our study's purpose here.

With  $P_{\text{succ}}$  now defined, we return to the question of whether a step-varying approach to  $p_s$  can improve gaussian amplitude amplification. For details on how an optimal  $p_s$  can be computed at each step of the algorithm, please see Appendix C for our technique. To summarize, we simulate a range of  $p_s$  values at each step, such that the distance in amplitude space between  $|P_{\min}\rangle$  and the mean (red 'x' in figures 8 and 9) is maximized, resulting in the largest reflection about the average from  $U_s$  per step. Figure 12 shows an example of this process for the case  $N = 30$ ,  $L = 4$ , and resulting  $P_M$  &  $P_{\text{succ}}$ .

As evidenced by the accompanying numbers in figure 12, a step-varying approach to  $p_s$  is indeed advantageous for getting the maximal peak probability out of a given  $W$ , and subsequently a higher  $P_{\text{succ}}$ . However, it is also clear that the exact sequence of  $p_s$  values (bottom plot) is non-trivial, and likely unpredictable from an experimental perspective when dealing with randomized data. The sharp fluctuations in  $p_s$  at every step, some small while others quite large, can be thought of as a signature of the  $W$  distribution, actively counteracting the randomness of the geometry at every step. Interestingly, the vast majority of  $p_s$  values are all right around 0.0105, the optimal single  $p_s$  value, with the notable exceptions being steps 1 – 20, around 600, and the final 100 steps.

The results shown in figure 12 were found by our simulations to be general. That is to say, *every* randomly generated  $W$  we studied, for all  $N$  and  $L$ , could always

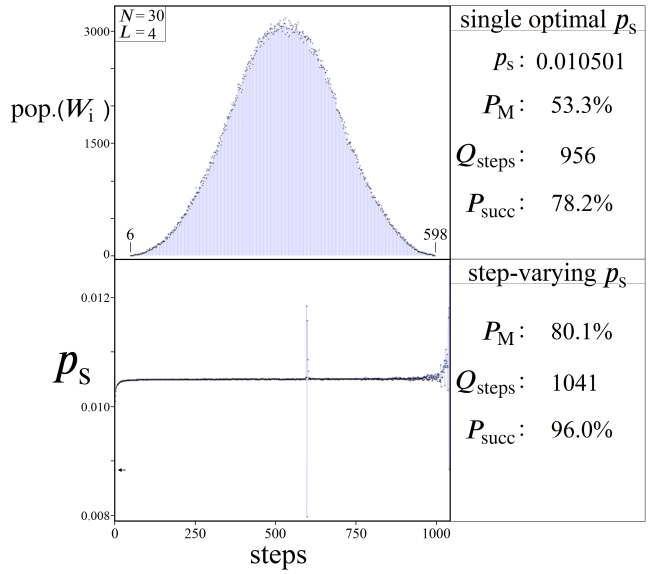


FIG. 12: (top) An example  $W$  distribution for the case  $N = 30$ ,  $L = 4$ ,  $R = 200$ . (bottom) A plot of all  $p_s$  values used at each step in order to optimized the probability of measuring  $|P_{\min}\rangle$ . Note the small black arrow, marking the  $p_s$  value at step 1. To the right of each plot are accompanying details about the success of amplitude amplification on  $W$ , using a single vs. step-varying  $p_s$  approach.

be optimized to produce a higher  $P_M$  using a step-varying  $p_s$  approach versus only a single  $p_s$  (see figure 13). Additionally, the three notable  $p_s$  exceptions mentioned above were also found with high regularity:  $p_s$  in the early steps are much lower (especially step 1), quickly gravitate towards the optimal single value for the majority of steps, plagued by very short periods of high fluctuation (interestingly, for larger sized problems these fluctuations happen with seemingly periodic structure), and finally a much slower fluctuation of values leading up to the peak  $P_M$ . Although we can't pinpoint an exact mathematical structure to explain all of these trends, the fact that nearly every single simulation showed these features is promising that there is indeed some underlying mechanism at work. And, if this process can be better understood, perhaps it could bring the step-varying  $p_s$  approach closer to experimentally realizable, instead of simply theoretical.

As a final note on the step-varying approach, in rare cases it was found that the larger  $P_M$  (as compared to the single optimal  $p_s$ ) did not directly translate to a better  $P_{\text{succ}}$ , as the resulting higher  $Q_{\text{step}}$  count caused  $P_{\text{succ}}$  to be lower. Additionally, for larger cases of  $W$  distributions which were discretized from perfect gaussians (eqn. 10), it was found that there was no difference between the single optimal  $p_s$  value and the step-varying approach (i.e. the step-varying approach yielded the same single  $p_s$  at every step). In general, our simulations found the step-varying  $p_s$  approach to be most effective at improving  $P_M$  and  $P_{\text{succ}}$  for smaller problem sizes. However, these

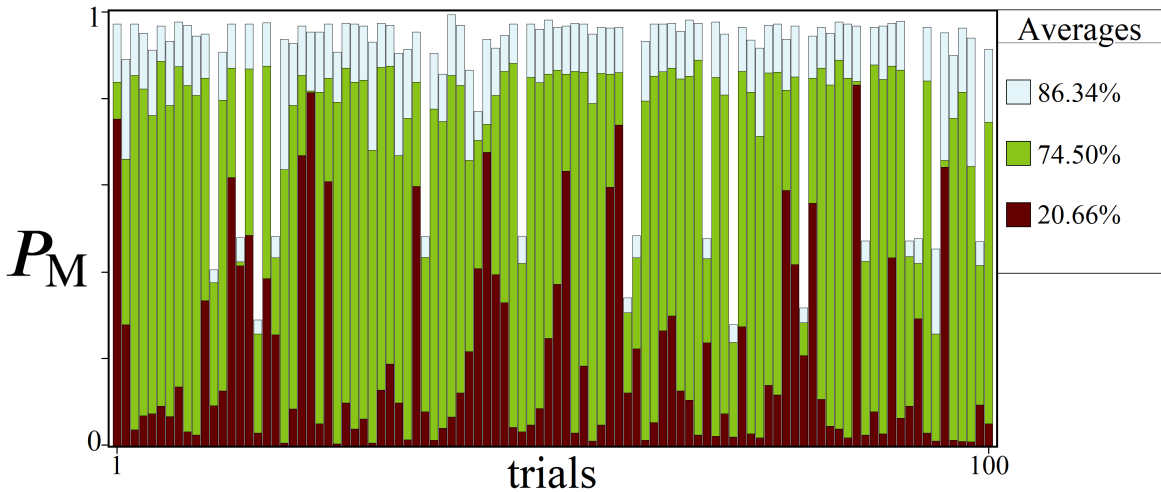


FIG. 13: Results from testing on 100 randomly generated  $\mathbb{W}$  distributions, for  $N = 6$ ,  $L = 10$ ,  $R = 100$ . For each trial, we report the highest  $P_M$  probability found for the state  $|P_{\min}\rangle$  using (light blue) a step-varying  $p_s$  approach, (green) a single optimal  $p_s$  approach, and (dark red) an average  $p_s$  approach. Reported on the right side of the figure are the averages found for all three approaches.

smaller cases oftentimes produced  $p_s$  vs. step plots such as figure 12 which were highly chaotic and irregular from problem to problem, even for the same  $N$  and  $L$ . Conversely, as problem sizes increase, the difference between the single vs. step-varying approaches becomes increasingly more negligible, with much more regular and stable  $p_s$  vs. step plots.

### C. Statistical Viability

While the results from the previous subsection can be thought of as leaning towards a more theoretical strategy for optimizing  $P_M$ , here we address the issue of finding  $p_s$  from a more practical perspective. In any realistic pathfinding or optimization problem, it is fair to assume that the solver has limited information about  $\mathbb{W}$ . Consequently, using a strategy for finding a suitable  $p_s$  such as equation 14 may be impossible, which begs the question: how feasible is gaussian amplitude amplification when used blindly?

In order to shed some light on this question, we've put together a statistical study, shown in figure 13, which illustrates the varying degrees of success one can expect using three different approaches. More specifically, the figure showcases 100 randomly generated  $\mathbb{W}$  distributions of size  $N = 6$ ,  $L = 10$ , and their resulting peak  $P_M$  probabilities. Optimal  $P_M$  values for each geometry were found through classically simulating amplitude amplification with 1) (light blue) a step-varying  $p_s$ , 2) (green) a single optimal  $p_s$ , and 3) (dark red) an average  $p_s$ . Details for the step-varying and single optimal  $p_s$  approaches can be found in the previous subsections. As for the average  $p_s$ , this value was computed by averaging together the 100 single optimal  $p_s$  values, which was approximately

$$p_s \approx 0.0083478.$$

Two noteworthy takeaways from figure 13 are as follows: 1) Even for this appreciably large problem size ( 60 million paths), about 15% of the  $\mathbb{W}$  distributions studied could not be optimized for  $P_M$  values over 50%. We found this to be of interest because it opens up the question: what is it about these  $\mathbb{W}$  distributions that makes them inherently difficult to boost? 2) The large discrepancy between the single optimal and average  $p_s$  plots can be seen quite clearly across the 100 trials. Returning to the question posed at the top of the subsection, these results suggest that blindly using gaussian amplitude amplification may be less than desirable for finding  $W_{\min} / W_{\max}$ . Cases where the average  $p_s$  approach yielded high  $P_M$ 's, nearing the optimal case, appear to be simply 'lucky', at least for this particular problem size.

Although the results shown in figure 13 do not support the viability of blind gaussian amplitude amplification, it is important to note that the figure does not tell the full story of what is happening with the remaining quantum states outside of  $|P_{\min}\rangle$ . Particularly for the average  $p_s$  cases, if the state  $|P_{\min}\rangle$  isn't receiving a large boost in  $P_M$ , perhaps another nearby state is, like the example in figure 11. If so, the viability of blind gaussian amplitude amplification may still hold some promise as a heuristic approach, perhaps even as a hybrid quantum/classical algorithm, or a learning-style algorithm such as QAOA [28, 29] or VQE [30].

### D. Other Problem Geometries

As the final topic of this study, we would like to reemphasize that the primary focus of this work is the idea of gaussian amplitude amplification, or more generally

any Phase Oracle  $U_P$  that can unlock new types of problems to solve using quantum computers. The pathfinding problem posed in figure 1 (sequentially connected bipartite graphs) was introduced as a motivation for the quantum circuits shown in figures 5 and 6, showcasing a complete problem. However, this geometry is quite specific, and the range of  $N$  and  $L$  values for which quantum is expected to outperform classical (high  $P_{\text{succ}}$ ) is small (high  $N$  and low  $L$  sized problems). For this reason, we present figure 14, which showcases two additional pathfinding problems, their underlying geometric structures, and example  $\mathbb{W}$  distributions.

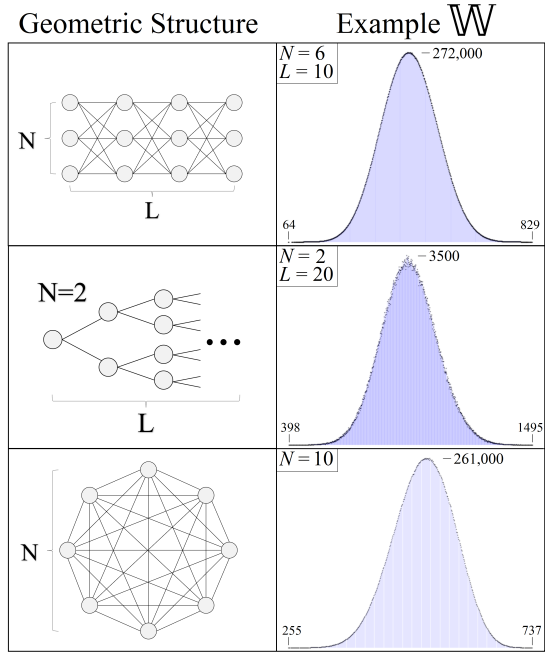


FIG. 14: (left) Three different classes of geometric structures on which pathfinding problems can be performed by assigning randomized weighted edges. (right) Classically generated example  $\mathbb{W}$  distributions for each geometry, all exhibiting gaussian-like structure.

The top geometry illustrated in figure 14 is once again the sequentially connected bipartite graph problem of sections II.-V., with an example  $\mathbb{W}$  distribution corresponding to the size studied in figure 13. In the center we have a Binary Spanning Tree geometry, illustrating a single case of a much larger class of tree-like models, and on the bottom we have a geometry with all-to-all connectivity, which is the underlying structure of the famed Traveling Salesman problem [27]. Most importantly, when we look at the space of all possible paths for each geometry ( $\mathbb{W}$ ), we once again find gaussian-like structure, with the solutions of interest  $W_{\min} / W_{\max}$  located on the tails.

Looking at the order in which the geometries in figure 14 have been presented, from top to bottom, there are two important trends when considering whether or not a quantum algorithm is applicable: potential for quantum speedup versus quantum circuit difficulty. In sections II.

and III. we covered how the sequentially connected bipartite graph can be efficiently translated into a quantum circuit for  $U_P$ . However, this efficiency is also advantageous for a classical solver, resulting in competing speeds on the order  $O(\sqrt{N^L})$  vs.  $O(N^2(L-1))$  (quantum vs. classical).

Focusing now on the Binary Spanning Tree, a classical pathfinding algorithm has less geometric structure to take advantage of, which consequently increases the expected classical solving speed up to the order  $O(2^L)$ , or more generally  $O(N^L)$ , where  $N$  is the number of spanning nodes per layer. On the other hand, the expected quantum solving speed remains unchanged, still on the order of  $O(\sqrt{N^L})$ , because  $N^L$  represents all possible paths which can be encoded into  $U_P$ . However, this increase in quantum speedup potential comes at the cost of the quantum circuit for  $U_P$ . In Appendix D we show one possible circuit design for  $U_P$ , but the gist of the problem boils down to a much higher demand on control gates and qubit connectivity.

Finally, the bottom geometry presented in figure 14, representing all-to-all connectivity, continues the two trends discussed above. For a geometry of  $N$  nodes, for which we would like to find the shortest possible path touching each node exactly once, the space of all possible paths has  $N!$  solutions. If one is able to encode such a  $\mathbb{W}$  into quantum states, then the expected solving speed would be  $O(\sqrt{(N!)})$ , which would be a tremendous success for quantum. However, creating a quantum circuit for  $U_P$  here is the most difficult of all three cases, plagued with several design challenges. Most notably, the space of all possible paths isn't naturally compatible with qubits. The phase oracle  $U_P$  for this problem needs to encode  $N!$  different phases onto a Hilbert Space of size  $2^Q$ , for which we see no straightforward approach.

Beyond the three geometries presented here, there are likely many more problems which give rise to solution spaces which are naturally gaussian-like. However, the challenge lies in finding these new problems, determining their potential for a quantum speedup, and ultimately implementing them into quantum circuits. We hope that the examples presented here spark further interest in gaussian amplitude amplification, and its potential use cases.

## VI. CONCLUSION

Amplitude amplification is a key ingredient for future success in quantum algorithms. The promise of quantum computers lies in the parallelism that superposition states have to offer, but converging these superposition states back down to a single answer is challenging. Twenty-five years ago, Grover demonstrated to the world a mechanism by which this is possible, igniting interest in quantum algorithms worldwide for over two decades (along with successes from many others). In this study, we hope to add to the success of amplitude amplification

by demonstrating a new problem type, namely pathfinding through a weighted geometry.

In sections II. and III., we outlined a pathfinding problem based on a geometry of sequentially connected bipartite graphs with weighted edges, provided a classical solving speed, as well as a translation of the problem into a quantum circuit. What follows in sections IV. and V. can be considered more general, applicable to any problem which naturally gives rise to a gaussian-like solution space. We demonstrate that Grover's Oracle operator  $U_G$  can be extended to a more general Phase Oracle  $U_P$ , and still cause interference effects which lead to high probabilities of measurement on desirable solution states. We show that  $U_P$  has potential for solving realistic problem cases involving randomness, highlighting not only the strengths of the quantum algorithm, but importantly its weaknesses as well.

### A. Future Work

The algorithmic potential for gaussian amplitude amplification presented in this study is a promising first step, but there is still much to be learned. From a purely mathematical perspective, we view the process illustrated in figure 9 as still not fully understood. Throughout the study we were able to simulate gaussian amplitude amplification classically because each Hilbert Space had a finite number of states. However, studying a continuous gaussian function as it undergoes  $U_s U_P$  through many steps is much more difficult, which we leave as an open question for future research. Additionally, studying the same process but with a skewed gaussian is likely even more challenging, but could yield highly valuable insight into more realistic problem cases, such as why certain  $W$  distributions in figure 13 performed better than others.

Finally, we believe that there are still undiscovered future problems that may be solvable with amplitude amplification, but are not strictly limited to gaussian-like solution spaces. Gaussian distributions arise naturally in large problem sizes, which not coincidentally is where quantum is expected to have the biggest potential over classical. However, just in the same manner by which one might be surprised to learn that a distribution such as figure 8 is capable of successful amplitude amplification, who knows what other sorts of distributions have potential as well (polynomial, exponential, etc.). The Phase Oracle  $U_P$  presented in this study is hopefully just one of many future optimization problems yet to be translated into amplitude amplification and solved using quantum computers.

### Acknowledgments

We gratefully acknowledge support from the National Research Council Associateship Program and Griffiss Institute. Any opinions, findings, conclusions or recom-

mendations expressed in this material are those of the author(s) and do not necessarily reflect the views of AFRL.

### Data & Code Availability

The data and code files that support the findings of this study are available from the corresponding author upon reasonable request.

---

[1] L. K. Grover, arXiv: 9605043 (1996)

[2] M. Boyer, G. Brassard, P. Hoyer, A. Tapp, *Fortschritte der Physik* **46** (1998)

[3] C. H. Bennett, E. Bernstein, G. Brassard, U. Vazirani, *SIAM Journal on Computing* **26** (1997)

[4] E. Farhi and S. Gutmann, *Phys. Rev. A* **57** (1998)

[5] G. Brassard, P. Hoyer, M. Mosca, A. Tapp, *AMS Contemporary Mathematics* **305** (2002)

[6] A. M. Childs and J. Goldstone, *Phys. Rev. A* **70** (2004)

[7] A. Ambainis, arXiv: 1010.4458 (2010)

[8] Prasanth Shyamsundar, arXiv: 2102.04975 (2021)

[9] R. L. Singleton Jr, M. L. Rogers, D. L. Ostby, arXiv: 2110.11163 (2021)

[10] S. Lloyd, *Phys. Rev. A* **61** (1999)

[11] G. F. Viamontes, I. L. Markov, J. P. Hayes, arXiv: 0405001 (2004)

[12] O. Regev, L. Schiff, arXiv:1202.1027 (2012)

[13] R. Seidel, C. K-U. Becker, S. Bock, N. Tcholtchev, I-D. Gheorge-Pop, M. Hauswirth, arXiv: 2110.07545 (2021)

[14] M. A. Nielsen, I. L. Chuang, *Quantum Computation and Quantum Information* pg. 249 (2000)

[15] G. L. Long, W. L. Zhang, Y. S. Li, L. Niu, *Commun. Theor. Phys.* **32** (1999).

[16] G. L. Long, Y. S. Li, W. L. Zhang, L. Niu, *Phys. Lett. A* **262** (1999).

[17] P. Hoyer, *Phys. Rev. A* **62** (2000)

[18] A. Younes, *Applied Mathematics & Information Sciences* **1** (2013)

[19] L. Tan, B. Wan-Su, L. Wen-Qian, Z. Hou, F. Xiang-Qun, *Chinese Phys. Lett.* **31** (2014)

[20] Y. Guo, W. Shi, Y. Wang, J. Hu, *Journal of the Physical Society of Japan* **86** (2017)

[21] P. H. Song, I. Kim, *Eur. Phys. Jour. D* **23** (2003)

[22] A. A. Pomeransky, O.V. Zhirov, D. L. Shepelyansky, *Eur. Phys. Jour. D* **31** (2004)

[23] J. Janmark, D. A. Meyer, T. G. Wong, *Phys. Rev. Lett.* **112** (2014)

[24] P. S. Laplace, *Mémoires de l'Académie Royale des Sciences de Paris*, **10** (1810)

[25] J. Bernoulli, *Ars Conjectandi*. Basileae: Thurnisiorum. (1713)

[26] C. F. Gauss, *Theoria Motus Corporum Coelestium in Sectionibus Conicis Solem Ambientium* (1809)

[27] K. Menger, *Zur Metrik der Kurven*, *Math. Ann.* **103** (1932)

[28] E. Farhi, J. Goldstone, S. Gutmann, arXiv:1411.4028 (2014)

[29] S. Hadfield, Z. Wang, B. O'Gorman, E. G. Rieffel, D. Venturelli, R. Biswas, *Algorithms* **12** (2019)

[30] A. Peruzzo, J. McClean, P. Shadbolt, M-H. Yung, X-Q. Zhou, P. J. Love, A. Aspuru-Guzik, J. L. O'Brien, *Nature Communications* **5** (2014)

[31] IBM 7-Qubit Casablanca and Lagos Architectures, <https://quantum-computing.ibm.com>. Accessed July - Aug. 2021

### Appendix A: $U_{ij}$ Circuit Design for $N = 4$

It is important to consider the impact of circuit design when pursuing cases of larger  $N$ . By comparing the quantum vs. classical expected solving speeds discussed in sections II. and IV.,  $O(\sqrt{N^L})$  vs.  $O(N^2(L-1))$ , one can derive that  $L \leq 4$  is where the quadratic speedup from quantum is expected to be most advantageous. Thus, in order to show how  $U_{ij}$  scales with  $N$ , here we present a circuit design for  $N = 4$ . Most notably, since there are now two qubits per layer, this requires higher order control-phase gates in order to properly apply the 16 weighted edges connecting layers  $i$  and  $j$ . In general, implementing any  $N = 2^n$  sized geometry will require all-to-all connectivity between neighboring layers of qubits.

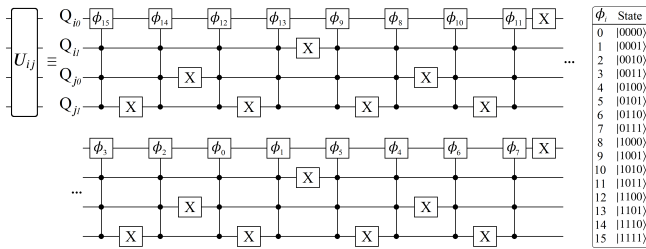


FIG. 15: Quantum circuit for achieving an  $N = 4$   $U_{ij}$  operation.

### Appendix B: $U_P$ Fidelity Results

Here we present experimental results which demonstrate the viability of implementing  $U_P$  on IBM's state-of-the-art qubit architectures 'Casablanca' and 'Lagos'[31]. Because  $U_P$  only applies phases (which are undetectable through measurements), each experiment consists of an application of  $U_P$  followed by  $U_P^\dagger$ , ensuring that each experiment has a definitive measurement result for calculating fidelity (the state of all  $|0\rangle$ 's). Equation B1 below shows the fidelity metric used.

$$f = \langle 0^{\otimes L} | H^{\otimes L} U_P^\dagger U_P H^{\otimes L} | 0^{\otimes L} \rangle \quad (B1)$$

Because of the multiplicative nature of fidelities, the actual fidelity of a single  $U_P$  application can be estimated as higher than the values shown in figure 16. Also note the dramatic decrease in fidelity between experiments  $L = 2$  and  $L = 3$ . This drop off can be explained by revisiting figure 6, and noting the difference in circuit depth for  $U_P$  when using 2 versus 3 qubits. For the special case of  $L = 2$ , we have  $U_P = U_{ij}$ , while for all other cases  $U_P$  requires two sets of  $U_{ij}$  operations. This difference in circuit depth explains the high fidelity for  $L = 2$  versus  $L = 3, 4, 5$ .

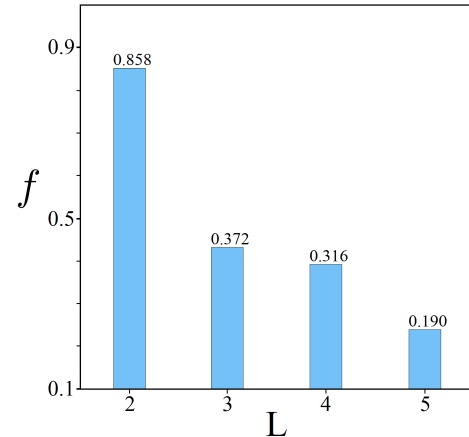


FIG. 16: Fidelity results as defined in equation B1, for the case  $N = 2$ ,  $L \in 2, 3, 4, 5$ , performed on IBM's superconducting qubits.

### Appendix C: Step-varying $p_s$

In order to compute the maximal  $P_M$  values displayed in figures 12 and 13, we used a classical simulation of the quantum state  $|\Psi\rangle$  at each step of the amplitude amplification process in order to determine optimal  $p_s$  values. Using each unique  $\mathbb{W}$  distribution, we were able to classically compute the complete set of  $N^L$  path lengths  $W_i$  and their corresponding path states  $|P_i\rangle$ . Then, at each step of the algorithm we test a range of  $p_s$  values when applying  $U_P$ , tracking the distance in amplitude space between the state  $|P_{\min}\rangle$  and collective mean, given in equation C2. Once a maximal  $D$  is found, the corresponding  $p_s$  value is stored, the diffusion operator  $U_s$  is applied to  $|\Psi\rangle$ , and the resulting probability  $P_M$  for  $|P_{\min}\rangle$  is recorded. Once the simulation finds a  $P_M$  value which is smaller than the previous step, the algorithm is terminated.

$$|\Psi\rangle = \sum_k^{N^L} \alpha_k |P_k\rangle$$

$$\text{Dist}(\alpha, \beta) \equiv \sqrt{\text{real}(\alpha - \beta)^2 + \text{imag}(\alpha - \beta)^2}$$

$$\alpha_{\text{mean}} = \frac{1}{N^L} \sum_k^{N^L} \alpha_k \quad (C1)$$

$$D = \text{Dist}(\alpha_{\text{mean}}, \alpha_{\min}) \quad (C2)$$

Figure 17 illustrates an example  $\mathbb{W}$  distribution, along with three  $p_s$  values and their effect on the states making up  $|\Psi\rangle$  at the first step. In each amplitude plot, the value of  $D$  and  $p_s$  are shown, along with a line connecting the locations of  $\alpha_{\min}$  and  $\alpha_{\max}$ . Carrying out the procedure described above leads to the largest  $P_M$  values reported in this study, but perhaps not necessarily the highest possible. We leave this as an open question for

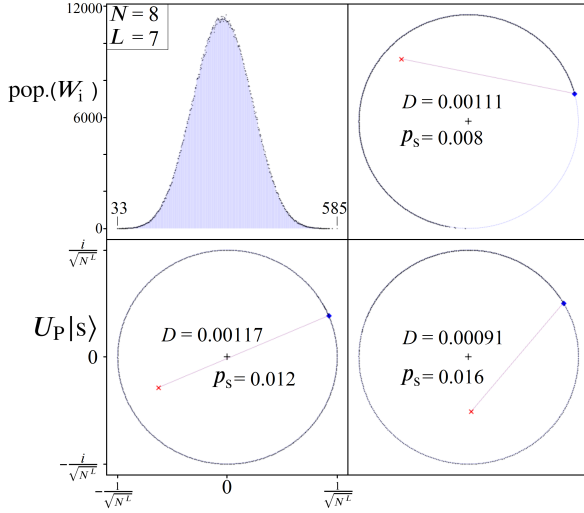


FIG. 17: Illustration of the classical simulation technique used to determine the optimal  $p_s$  value at each step.

future research, as to whether or not another procedure for determining a step-varying  $p_s$  approach could result in better probabilities for measuring  $|P_{\min}\rangle$ . If so, it would mean using lower  $D$  values at some intermediate steps in

order to reach a higher  $P_M$  overall, which would be quite interesting.

#### Appendix D: Binary Spanning Tree Circuit

To illustrate that other geometries can be translated into quantum pathfinding problems, we present figure 18 below, showcasing a binary spanning tree geometry ( $N = 2, L = 3$  from the early discussion regarding figure 14). Each edge in the geometry is assigned a randomized weight  $\omega_i$ , which is then converted into phases  $\phi_i$  for phase gates, via an appropriate scaling factor  $p_s$ .

Similar to the quantum circuit design presented in figures 5 and 6, we once again have a one-to-one phase gate count per weighted edge in the geometry. However, where the circuitry for sequentially connected bipartite graphs excelled in parallelism, only requiring  $N^2 \cdot (L - 1)$  phase gates in order to produce  $N^L$  unique phases, here we need  $\sum_{i=1}^L 2^i$  phase gates in order to pathfind on a geometry of only  $2^L$  paths. Since the number of phase gates exceeds the total paths count, as well as requiring connectivity and  $L$ -order control between qubits, implementation of this particular geometry is less likely to find success on near term quantum computers.

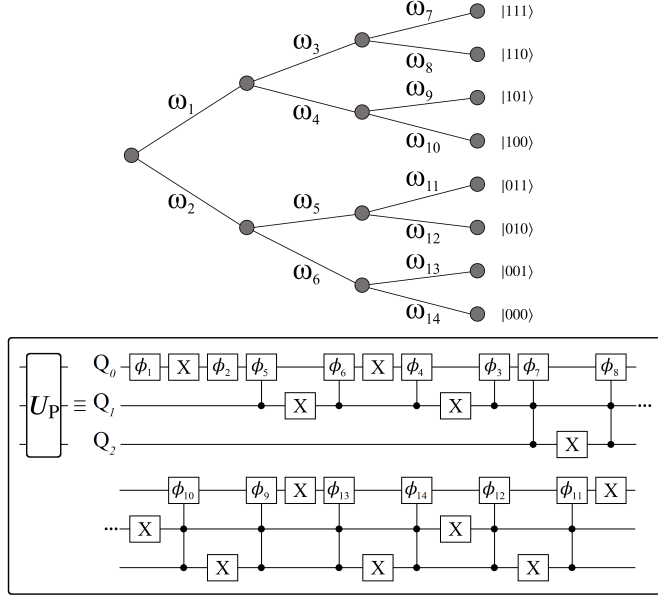


FIG. 18: (top) Geometry of a binary spanning tree with weighted edges, for  $L = 3$ . Quantum states for each full path are shown next to the rightmost layer. (bottom) A quantum circuit for implementing the Phase Oracle  $U_P$ , where each phase gate  $\phi_i$  corresponds to a weighted edge  $\omega_i$  in the geometry.